MRI Based Injury Characterization Immediately Following Ablation of Atrial Fibrillation

JJE Blauer[1,2], J Cates[1,2], CJ McGann[1], EG Kholmovski [1], A Alexander[2], MW Prastawa [2], S Joshi [2], NF Marrouche [1], RS MacLeod[1,2]

[1] CARMA Center, University of Utah, Salt Lake City, Utah, USA
[2] SCI Institute, University of Utah, Salt Lake City, Utah, USA

Abstract

A major limitation of catheter ablation for atrial fibrillation is the lack of tools to evaluate the efficacy and extent of lesion creation. Late gadolinium enhanced MRI has been used to detect acute injury following ablation, and scar tissue that forms weeks to months later. However, at the earliest imaging time point previously feasible in a clinical setting (< 24 hrs. post-ablation) the tissue hyperenhancement was diffuse and poorly predictive of future scarring. Using a new EP/MRI facility, and images acquired approximately 1 hr. post-ablation, heterogeneous atrial wall enhancement was observed. Specifically, regions of hypo-, normal, and hyper-enhancement were detected. Quantitative comparison of hyper-enhancing scar at 3 months post-ablation to enhancement states imaged acutely indicated a significant majority of scar comes from hypo-enhancing tissue. Further study of hypo-enhancing tissue may facilitate early examination of procedural endpoints and prediction of scar formation.

1. Introduction

Atrial fibrillation (AF) is the most common medically relevant cardiac arrhythmia. Over the past decade many non-pharmacological treatments for atrial fibrillation have emerged, with much attention focusing on intracardiac catheter ablation (ICCA). During an ICCA procedure for AF anatomical structures are targeted for ablation in an attempt to electrically isolate rouge activation pathways. To this end, numerous technologies have been implemented clinically to improve the efficacy and safety of ablation procedures, including catheter steering and sensing devices, and anatomical imaging modalities. While these technologies have improved the ability of operators to position catheters during ICCA, they provide little insight into the extent of ablation induced tissue modification. Thus, without knowing which ablation lesions will result in conduction blocking scar some lesion sets are insufficient to isolate pathological electrical sources [1].

Cardiac MRI has advanced to the point that residual scarring in the atria from ICCA for AF can be visualized using late gadolinium enhanced (LGE) MR imaging[2]. Results from studies using LGE MRI to assess atrial scar formation confirm that location and extent of scar formation are predictive of freedom from recurring AF[3, 4]. However, this data, acquired weeks to months post-ablation, has little immediate clinical utility. LGE MRI at early time points following ablation (< 24 hrs.) has been reported on, but this study found that early gadolinium enhancement was poorly predictive of scarring at 3 months post-ablation[5].

Access to an EP-MRI laboratory, a traditional fluoroscopy suite with an immediately adjoining 3 Tesla MRI, at the University of Utah Medical Center has recently facilitated the acquisition of LGE MRIs of patients immediately following (approximately 1 hr.) radio frequency ICCA. Examination of these images yielded regions of enhancement in the atrial wall, as expected, and also unanticipated dark regions (Figure 1). Reminiscent of ventricular no-reflow injury seen in myocardial infarct, and contrast voids from ventricular ablation studies, it was hypothesized that these dark regions represented tissues directly targeted by ablation to the extent that microvascular blood
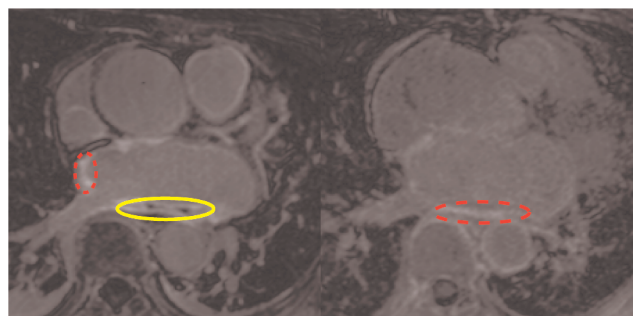

Figure 1. LGE MRI images acquired IPA (L) and 3PA (R). Dark regions (hypo-enhancment) of atrial tissue observed IPA (solid ellipse) hyper-enhancement (dashed ellipses).

flow had been terminated and contrast agent was no longer able to perfuse into the region[6, 7]. However, invasive histological evaluation was impossible to confirm this hypothesis. In leu of histological examination, we compared the enhanced and dark regions observed immediately post ablation (IPA) to scarring as seen in routine follow-up LGE MRI images acquired 3 months post ablation (3PA).
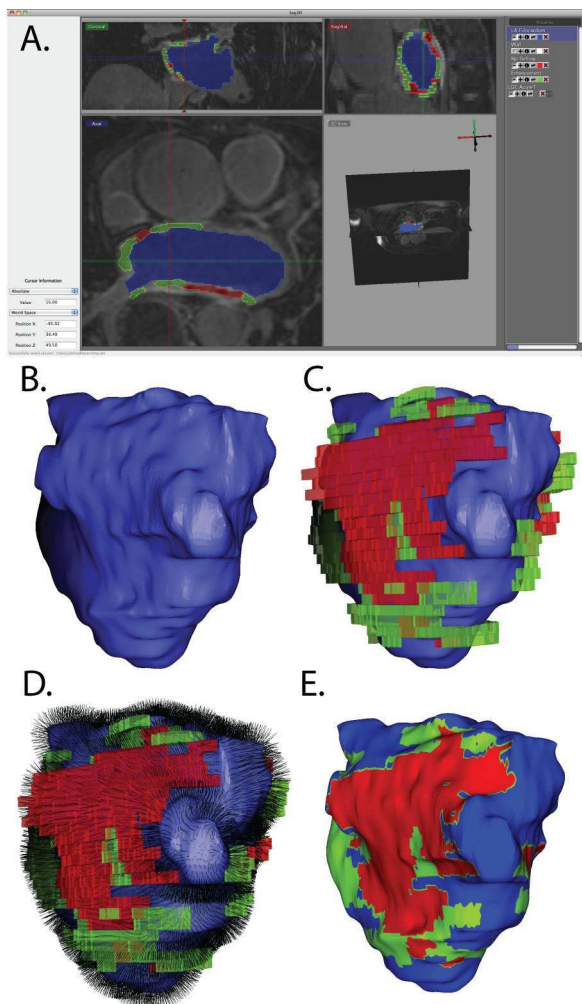

Figure 2. Creation of surface model for display and analysis of tissue enhancement states. (A.) The endocardial surface of the left atrium (blue), along with regions of the LA wall with different enhancement states (red→hypo-enhancement and green→hyper-enhancement) were defined using Seg3D. (B.) A surface model generated from the segmentation of the endocardial surface. (C.) Addition of isovolumes generated from the tissue type segmentations (D.) Samples of the surrounding isovalues were recorded at discrete intervals (.2 mm) along normal vectors extending from the surface of the mesh 4 mm into the surrounding space. (E.) The maximum isovalue detected along normals mapped to the nodes on the model.

We hypothesize that characterization of atrial tissue with delayed uptake of contrast IPA will have predictive value for future scar formation and thus provide a new metric to develop effective procedural endpoints. Here we report our methodology and findings of this comparison from a cohort of 10 patients.

2. Methods

10 patients receiving catheter ablation for AF underwent MR imaging at IPA and 3PA time points. All patient procedures were performed in our EP-MRI suite in a manner previously described [3, 5]. As part of the MR imaging repertoire high resolution LGE images were acquired 15+/-3 minutes after injection of 0.1 mmol/kg gadolinium contrast agent (Multihance, Bracco Diagnostics Inc., Princeton, NJ) using a 3D respiratory navigated, inversion recovery prepared GRE pulse sequence with TR/TE = 1.4/3.1 ms, flip angle of $13°$, bandwidth = 710 Hz/pixel, FOV = 400 x 400 x 110 mm, matrix size = 320 x 320 x 44, 9% oversampling in slice encoding direction, voxel size = 1.25 x 1.25 x 2.5 mm, phase encoding direction: left to right, fractional readout = 87.5%, partial Fourier acquisition: 80% in phase-encoding direction and 90% in slice-encoding direction, GRAPPA with R = 2 in phase encoding direction. Inversion pulse was applied every heart beat and fat saturation was applied immediately before data acquisition. Data acquisition was limited to 15% of RR cycle and was performed during LA diastole. To preserve magnetization preparation in image volume, navigator was acquired immediately after data acquisition block. Typical scan time for LGE study was 4-8 minutes depending on heart rate and respiration pattern.

All LGE images were processed to delineate the geometry of the endocardial surface of the left atrium (LA), and to differentiate normal versus hyper-enhancing (IPA and 3PA) and hypo-enhancing tissue (IPA only, no hypo-enhancement was observed at 3PA time point). Specifically, manual segmentation of these regions of interest was performed by 2 expert operators using Seg3D. The segmentation of the endocardial boundary was then imported into SCIRun to generate a 3D surface model of the LA anatomy. Subsequently, the binary volumes of the hyper, and hypo-enhanced tissues were loaded into the same space as the LA surface model with the value of 1 or 2 written to regions labeled hyper or hypo enhanced (respectively), and 0 everywhere else. Normal vectors to the surface at each node on the model were then calculated, along which regularly spaced increments (20) to the depth of 4 mm were used to sample the isovalues of the binary volumes both inward and outward from the surface node. A scheme was implemented such that the maximum isovalue detected along the sample range for a given node was then assigned to that node.

Comparison of IPA to 3PA enhancement patterns is complicated by the inherent need for the registration of data acquired at two different time points and recorded at locations on representative surfaces differentiated by position, motion, and swelling. Initially, the differences associated with positioning were removed using a rough manual alignment of the meshes in SCIRun. However, ablation of the LA wall results in substantial swelling of the cardiac tissue and deformation in the LA geometry as observed IPA. Therefore, an additional non-ridgid mapping should be used to align corresponding regions to remove bias from the geometric differences due to swelling and motion. To overcome these challenges we selected a deformable surface matching registration algorithm [8]. This algorithm allowes a closest match of the endocardial surface mesh

to be determined without *a priori* definition of true correspondence.

The surface matching algorithm solves for a smooth deformation h between the IPA and 3PA surfaces by posing it as a minimum mean square error estimation problem [9]. This approch uses a correspondence free metric between the nodes on each surface such that the squared difference between two surfaces is defined as

$$d^2(S_1, S_2) = \frac{1}{N^2} \sum_{i,j}^{N} k(x_i, x_j) -$$
$$\frac{2}{NM} \sum_{i=1}^{N} \sum_{j=1}^{M} k(x_i, y_j) +$$
$$\frac{1}{M^2} \sum_{i,j}^{M} k(y_i, y_j,) \tag{1}$$

where x and y represent the 3-D coordinate in each surface and the total number of nodes are N and M respectively. A gaussian kernel k is used with a scale parameter sigma. The desired mapping is the solution to the subsequent minimization problem

$$h = \underset{h}{\operatorname{argmin}} \, d^2(S_1, S_2 \circ h)/labeleq2 \tag{2}$$

This algorithm solves the minimization problem with a greedy gradient decent and was ran for 600 iterations with three kernel scales which resulted in sufficinet convergnece for every patient. The first 300 iterations were with a kernel width of 10 immediately followed by 200 iterations with a kernal width of 7, and finally, 100 iterations with a kernal width of 5. At each iteration, regularization was applied with a gaussian kernel width of 10.

Following registration, the tissue classification values that had been previously calculated for the 3PA mesh were interpolated onto the IPA mesh using a nearest neighbor interpolation scheme (Figure 3). With the 3PA values mapped to the IPA surface, a point by point comparison of local tissue type at both time points was possible. This comparison was carried out by calculating the percent of each tissue type at IPA that became hyper-enhancement (scar) at 3PA, and subsequently by calculating the amount of scar composed of tissue previously classified as normal, hyper, or hypo-enhanced.

A refinement of this analysis was also performed in which regions that are difficult to segment due to partial volume effects, or motion artifact were omitted from the analysis. The regions omitted included the left atrial appendage, roof, and mitral valve regions. Statistical analysis was performed using a Student's t-test with Bonferroni correction for multiple comparisons. A p-value of less than 0.05 was considered significant.
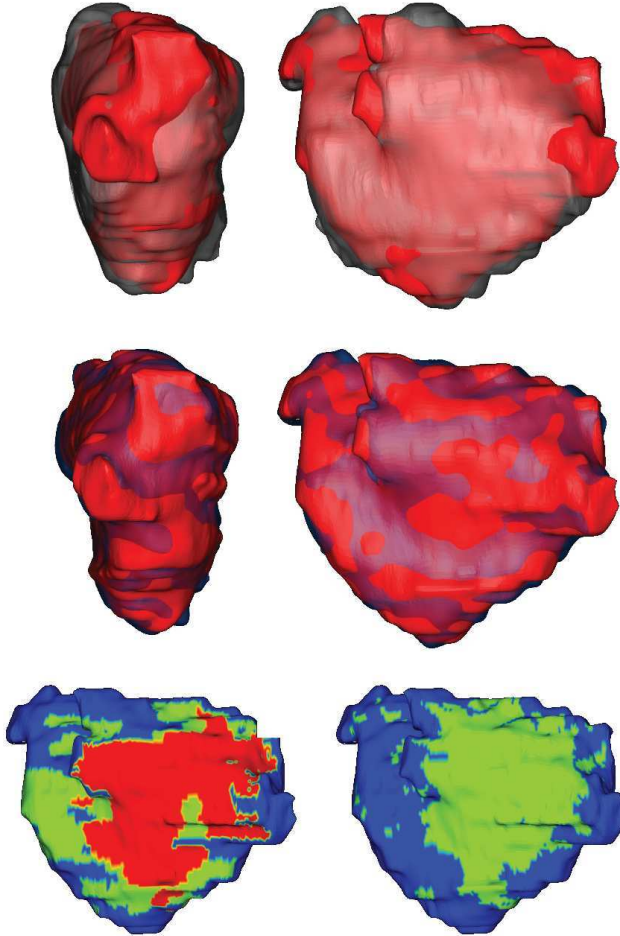

Figure 3. Registration of 3PA surface model to IPA model. (Top) The 3PA model (transparent) rigidly aligned to the IPA model (solid). (Middle) Deformable registration of the 3PA surface to the IPA surface. (Bottom) Image data originally mapped onto the 3PA surface model interpolated onto the IPA surface model (R) for comparison with the IPA mapping (L). surface mesh.

Table 1. Classification of Enhancement States in IPA and 3PA LGE MRIs. The percent of the entire LA wall (ELA), and the refined analysis region (RLA) composed of each type of tissue enhancement (hypo, normal, and hyper-enhancement).

State	Normal	Hyper	Hypo
ELA IPA	54.4±9.7%	28.2±6.9%	17.4±6.6%
ELA 3PA	80.0±8.2 %	20.0±8.2%	N/A
RLA IPA	27.8±13.0%	36.3±10.9%	35.9±14.8%
RLA 3PA	64.0±11.1%	36.0±11.1%	N/A

Table 2. Percentage of scar originating from each enhancement state IPA.

Tissue Type	Entire LA	Refined LA
Normal	$21.1 \pm 7.7\%$	$10.5 \pm 5.5\%$
Hyper	$32.6 \pm 11.2\%^{*}$	$30.6 \pm 15.3\%^{*}$
Hypo	$46.3 \pm 16.3\%^{*}$	$59.0 \pm 19.4\%^{*\dagger}$

* Significantly different from Normal ($p < 0.05$)
† Significantly different from Hyper ($p < 0.05$)

3. Results

Hypo and hyper-enhancement were observed in all 10 patients undergoing LGE-MRI immediately following ablation. Additionally, hyper-enhancement was observed in all 3PA LGE-MRI scans. For the IPA LA as a whole nearly half of tissue (43.6%) was label as either hypo, or hyper-enhanced (Table 1). Subsequently, in the 3PA LA hyper-enhancement accounted for about half as much of the tissue (20%), indicating a resolution of some of the injury seen IPA. This trend is also observed in the refined LA.

The percentage of scar (hyper-enhancment at 3PA) originating from each IPA tissue type was calculated, and the most common source was tissue that hypo-enhanced IPA. This is significantly more than the percentage of scar originating from either the normal or hyper-enhanced tissue IPA (Table 2). This trend strengthened in the refined analysis of the LA tissue.

4. Discussion and conclusions

This study shows that while the amount hypo-enhancement is less than that of both normal and hyper-enhancing tissue, or proportional in the refined analysis, the amount of scar originating from this tissue is greater than the other tissue types. This finding points towards hypo-enhanced tissue as the most likely candidate for prediction of scarring.

This data and subsequent analysis constitute an original and preliminary examination of the ability of MRI to classify early injury following ICCA of AF. Many opportunities for optimization and validation of this workflow exist. Important targets for optimization include establishing the best time post contrast injection for acquisition of the LGE MRIs, moving beyond manual classification of tissue type, and validating the use of the registration algorithm for this particular data. In spite of these limitations, these early results warrant future study of the role of hypo-enhancing tissue IPA.

In current clinical practice evaluation of lesion formation is wholly dependent on electrophysiological parameters. While these parameters are indicative of lesions having been formed they provide little insight about the extent, or completeness of lesion sets. The workflow proposed by this study suggests that image features extracted from LGE MRIs immediately following ablation may permit early and improved analysis of ablation lesions. In particular, the ability to predict the extent and completeness of scar formation would have significant clinical impact.

References

[1] Verma A, Kilicaslan F, Pisano E, et al. Response of atrial fibrillation to pulmonary vein antrum isolation.... Circulation Aug 2005;112(5):627–35.

[2] Peters DC, Wylie JV, Hauser TH, et al. Detection of pulmonary vein and left atrial scar after catheter ablation.... Radiology Jun 2007;243(3):690–5.

[3] McGann CJ, Kholmovski EG, Oakes RS, et al. New magnetic resonance imaging-based method for defining the extent of left atrial wall injury.... Journal of the American College of Cardiology Oct 2008;52(15):1263–71.

[4] Taclas JE, Nezafat R, Wylie JV, et al. Relationship between intended sites of rf ablation.... Heart rhythm the official journal of the Heart Rhythm Society Apr 2010;7(4):489–96.

[5] Badger TJ, Oakes RS, Daccarett M, other. Temporal left atrial lesion formation after ablation of atrial fibrillation. Heart rhythm the official journal of the Heart Rhythm Society Feb 2009;6(2):161–8.

[6] Rogers WJ, Kramer CM, Geskin G, et al. Early contrast-enhanced mri predicts late functional recovery.... Circulation Feb 1999;99(6):744–50.

[7] Dickfeld T, Kato R, Zviman M, et al. Characterization of radiofrequency ablation lesions.... Journal of the American College of Cardiology Jan 2006;.

[8] Glaunes J, Trouve A, Younes L. Diffeomorphic matching of distributions.... CVPR 2004;2:712–8.

[9] Glaunes J, Joshi S. Template estimation from unlabeled point set data and surfaces for computational anatomy. Proc of Workshop MFCA 2006;.

Address for correspondence:

Joshua Blauer
blauer@sci.utah.edu